ARL-TR-9280 ● SEP 2021

Development of Objective Go/No-Go Criteria for Determining the Electrostatic Sensitivity of Novel Metal Additives

by Kristi N Naude, Elliot R Wainwright, Lily Giri, and Jennifer L Gottfried

NOTICES

Disclaimers

The findings in this report are not to be construed as an official Department of the Army position unless so designated by other authorized documents.

Citation of manufacturer's or trade names does not constitute an official endorsement or approval of the use thereof.

Destroy this report when it is no longer needed. Do not return it to the originator.

ARL-TR-9280 ● SEP 2021

Development of Objective Go/No-Go Criteria for Determining the Electrostatic Sensitivity of Novel Metal Additives

Jennifer L Gottfried and Elliot R Wainwright
Weapons and Materials Research Directorate,
DEVCOM Army Research Laboratory

Kristi N Naude
Texas A&M University

Lily Giri
Bennett Aerospace, Inc.

REPORT DOCUMENTATION PAGE

Form Approved
OMB No. 0704-0188

1. REPORT DATE *(DD-MM-YYYY)*	2. REPORT TYPE	3. DATES COVERED (From - To)
September 2021	Technical Report	June 2021 – August 2021

4. TITLE AND SUBTITLE
Development of Objective Go/No-Go Criteria for Determining the Electrostatic Sensitivity of Novel Metal Additives

5a. CONTRACT NUMBER

5b. GRANT NUMBER

5c. PROGRAM ELEMENT NUMBER

6. AUTHOR(S)
Kristi N Naude, Elliot R Wainwright, Lily Giri, and Jennifer L Gottfried

5d. PROJECT NUMBER

5e. TASK NUMBER

5f. WORK UNIT NUMBER

7. PERFORMING ORGANIZATION NAME(S) AND ADDRESS(ES)
DEVCOM Army Research Laboratory
ATTN: FCDD-RLW-WA
Aberdeen Proving Ground, MD 21005

8. PERFORMING ORGANIZATION REPORT NUMBER
ARL-TR-9280

9. SPONSORING/MONITORING AGENCY NAME(S) AND ADDRESS(ES)

10. SPONSOR/MONITOR'S ACRONYM(S)

11. SPONSOR/MONITOR'S REPORT NUMBER(S)

12. DISTRIBUTION/AVAILABILITY STATEMENT
Approved for public release: distribution unlimited.

13. SUPPLEMENTARY NOTES
ORCID ID(s): Jennifer Gottfried, 0000-0002-1282-1928; Elliot Wainwright, 0000-0002-2301-9420

Kristi Naude was sponsored by the Army Research Laboratory under Cooperative Agreement Number W911NF21-2-0114.

14. ABSTRACT
Diagnostic instruments such as high-speed cameras and photodiodes were added to an electrostatic discharge (ESD) device. In addition to the integrated infrared emission from the combusting particles, the aluminum monoxide emission from reacting aluminum samples was recorded for each discharge event. The capacitance and voltage settings were selected to minimize electronic noise in the diagnostic equipment. The ESD energy was varied to determine the minimum ignition energy (i.e., electrostatic sensitivity) of two exemplar modified aluminum nanoparticle samples. This data was used to select objective criteria for determining whether each discharge event successfully ignited the sample ("go") or not ("no go"). The use of objective criteria based on amplified detectors rather than visual observation of combustion subject to operator interpretation will enable the determination of the electrostatic sensitivity of novel reactive materials under development using small quantities of the powdered samples. Thus, the electrostatic properties of the materials can be tailored to meet military specifications early on in the development process, prior to scale-up and formulation for large-scale testing.

15. SUBJECT TERMS
electrostatic discharge, ESD, aluminum, graphene oxide, ignition, sensitivity, aluminum monoxide, emission

16. SECURITY CLASSIFICATION OF:			17. LIMITATION OF ABSTRACT	18. NUMBER OF PAGES	19a. NAME OF RESPONSIBLE PERSON
a. REPORT	b. ABSTRACT	c. THIS PAGE			Jennifer Gottfried
Unclassified	Unclassified	Unclassified	UU	26	19b. TELEPHONE NUMBER (Include area code) 410-278-7573

Contents

List of Figures iv

List of Tables iv

1. Introduction 1

2. Experimental Setup 3

3. Optimization of Experimental Parameters 4

3.1 ESD-Related Settings 4

3.2 Diagnostic-Related Settings 5

4. Summary of Calibrated Experimental Settings 8

5. Recommended Criteria for Determining Go/No-Go 10

6. Application of Methodology to Samples of Interest 11

7. Discussion and Conclusions 14

8. Future Work 15

9. References 17

List of Symbols, Abbreviations, and Acronyms 19

Distribution List 20

List of Figures

Fig. 1 Criteria for current go/no-go determination 1

Fig. 2 a) ESD electrode and sample stage schematic and b) photograph of the Electro-Tech Systems Model 931 Firing Test System 3

Fig. 3 Experimental schematic of the ESD system and additional diagnostics 4

Fig. 4 PD signal from the ESD generated on blank carbon tape at 625 mJ 7

Fig. 5 Comparison of "go" vs. "no-go" optical signals for a highly sensitive sample; emission observed at times greater than 0.3 ms (green dashed line) indicates successful particle ignition/combustion ("go") 10

Fig. 6 SEM images of commercial nano-Al (left) and commercial GO (right) 11

Fig. 7 Snapshot from the high-speed video of physically mixed nano-Al+GO sample burning 3.0 ms after ESD ignition at 10 mJ (picture has been cropped and the brightness/contrast adjusted) 12

Fig. 8 AlO (left) and IR (right) PD traces for the physically mixed nano-Al+GO sample 12

Fig. 9 SEM images of GO-coated nano-Al at 20,000× (left) and 50,000× (right) 13

Fig. 10 AlO (left) and IR (right) PD traces for the GO-coated nano-Al sample 13

Fig. 11 Snapshot from the high-speed video of GO-coated nano-Al particles being ejected into the air 30 μs after being subjected to a 10.5-J discharge; the ejected particles appear black against the residual discharge emission since they are not burning, while a few smaller particles inside the yellow circle may be burning (picture has been cropped and the brightness/contrast adjusted) 14

Fig. 12 Proposed multistep electrostatic sensitivity testing regime for novel metal additives 16

List of Tables

Table 1 Experimental apparatus settings under different discharge conditions 9

1. Introduction

The creation of next-generation munitions requires novel additive materials (e.g., Jiang et al.[1]) to increase performance while ensuring safe operation. Current DOD standard methods[2] for characterizing energetic material electrostatic sensitivity (i.e., the tendency to ignite when subjected to an electrostatic discharge [ESD]) rely on inherently subjective criteria and are designed for conventional monomolecular military explosives consisting primarily of carbon (C), hydrogen (H), nitrogen (N), and oxygen (O). This methodology involves taping a sample of the material to a measurement stage and then subjecting it to an ESD of specified energy. The presence of sufficient cracks in the tape is then used to confirm the ignition (go) or non-ignition (no-go) of the sample, the subjectivity of which is shown in Fig. 1. This procedure consequently relies on fallible human determination to classify the sensitivity of novel energetic materials, rather than being grounded in objective standards. To pass the sensitivity test, the energy required to ignite the sample must be equal to or higher than a similar previously qualified material. For example, the ESD sensitivity of novel CHNO explosives is compared to RDX.[3] Presently, such a baseline material has not been universally established for metallic additives.

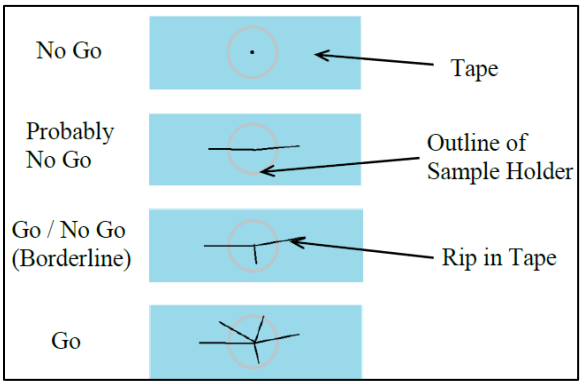

Fig. 1 Criteria for current go/no-go determination[4]

The appropriate criteria for determining the electrostatic sensitivity of nonconventional novel reactive materials (e.g., thermite-like pyrotechnic compositions of two or more nonexplosive solid materials that stay inert and do not react with each other until subjected to a sufficiently strong stimulus) require development, as metal-based reactive materials are known to be more sensitive to ESD than conventional organic-based energetic materials.[5] Recent efforts to study novel metallic additive electrostatic sensitivity are influenced by the same subjectivity as the currently employed DOD standard methods. Prof Michelle Pantoya's group at Texas Tech University has investigated the electrostatic sensitivity of a number of reactive materials. In a study conducted by Steelman et

al.,[6] mixtures of aluminum (Al) and copper oxide (Cu_2O) nanoparticles doped with a carbon nanotubes (CNTs) were examined. Only 0.1-J discharges were tested, and no criteria were provided for confirming a sample's combustion, other than stating that "ESD testing clearly resulted in ignition or no ignition." [6] Similarly, micron-sized particles of Al and Cu_2O mixed with CNT were studied by Poper et al.[7] While in this study they varied the discharge energies in order to determine the sample's specific ignition threshold, the same statement concerning the definitive nature of a sample's "ignition or no ignition" was made. Weir et al.[5] likewise tested micron-sized Al mixed with various metals, metal oxides, or fluoropolymer at varying discharge energies but made no mention of the criteria used to confirm sample ignition; a similar study by the same group investigated the effect of particle size on the electrostatic sensitivity.[8]

Prof Edward Dreizin's group at the New Jersey Institute of Technology has also studied the ignition of metal particles via ESD. The ignition of Al powders at four different discharge energies was studied to elucidate the mechanisms for powder ejection and ignition.[9] Although emission traces of burning particles were acquired by photodiode (PD) to determine burn times, the discharge voltages were selected to ensure particle ignition occurred and no threshold for ignition was determined. They subsequently performed a similar study to determine the effect of the thickness of layers of Al, magnesium (Mg), or titanium (Ti) powders.[10] The ignition delays for thermites of Al with CuO or MoO_3 were studied, and the minimum ignition energies were determined "based on visual detection of ignition."[11] Photographs of the electrostatic ignition of various Al-based thermites were used to measure parameters such as the distance the burning particles travelled.[12] The displacement and de-agglomeration of Mg powders by the shock wave generated from an ESD was investigated,[13] as was the mechanism for ignition of zirconium (Zr) powders.[14]

The group at the French-German Research Institute of Saint-Louis has investigated the use of nanodiamond to reduce the electrostatic sensitivity of Al/Bi_2O_3 thermites.[15] They stated that the electrostatic threshold was defined as "the minimum [energy] required for observing at least one positive pyrotechnic reaction in six tests."[15] More recently, they investigated the use of a conductive polymer for densensitizing Al/SnO_2 thermites citing the criteria of the presence of "fumes, sound, luminous flash, change of powder aspect, etc." to determine go/no go events.[16,17] Purdue's ESD system also relies on "any audible combustion noise, visible flame, and or burnt product material" to identify ignition events—a comparison of the 50% energy threshold for commercial 80-nm Al determined on their system (2.5 mJ), and a similar instrument at China Lake (1.2 mJ) showed a greater than 50% difference in the threshold value.[18]

Relying on the operator's visual observation of burning particles is a subjective technique that may result in the determination of different ignition thresholds by different operators. In addition, the need to see the emission by eye (or definitive cracks on the tape substrate) necessitates using larger sample sizes to make the combustion event more obvious. Since novel metal additives in the US Army Combat Capabilities Development Command Army Research Laboratory's laboratories and those of our collaborators are often produced in very small quantities initially (milligram batch sizes), a more sensitive method for detecting particle combustion is desired. Thus, the development of a sensitive, objective method for quantifying novel reactive material electrostatic sensitivity using a minimal amount of material is required to ensure repeatability, accuracy, and end users' safety prior to scale-up and formulation for large-scale performance testing.

2. Experimental Setup

The experimental setup used to develop objective electrostatic sensitivity evaluation criteria utilizes an Electro-Tech Systems Model 931 Firing Test System D ESD device (Fig. 2). This system enables fine control of the discharge energy in increments of 1 mJ or larger, depending on the size of capacitor used. The larger capacitors (such as 0.5 μF) only allow increments of several joules but provide the additional benefit of allowing higher-energy discharges, up to a maximum of 15.75 J. The system includes a firing test chamber with a 15- × 10-cm polycarbonate window to enable viewing and diagnostic access. For ESD tests, the material is placed on the grounded sample holder, which is then raised to within close proximity of the needle electrode.

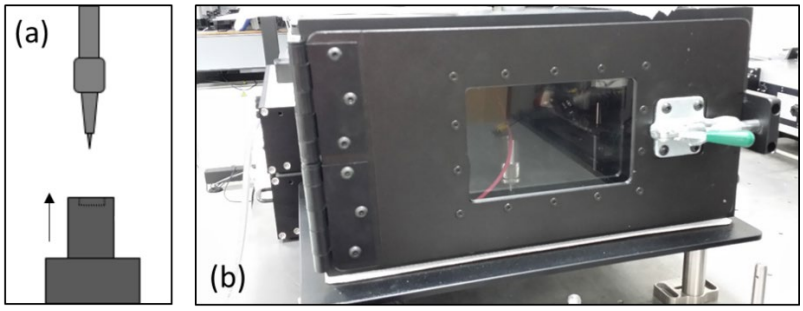

Fig. 2 a) ESD electrode and sample stage schematic and b) photograph of the Electro-Tech Systems Model 931 Firing Test System

For this work, the diagnostic instruments included two New Focus PDs: Model 2051 for the visible 300- to 1100-nm range and 2053 for the IR 800- to 1800-nm range, with a New Focus Model 0901 external power supply. The various filters used with these PDs are described below. Two FASTCAM Mini AX200 high-speed

cameras were aligned to image the same field of view (using a 50:50 beamsplitter); the two cameras could be used to effectively double the maximum frame rate, to perform high dynamic range imaging,[19] or to obtain two-color optical pyrometry measurements.[20] An Agilent Technologies InfiniiVision DSO7104A oscilloscope was used to record the voltage signals from the PDs, which were subsequently used to trigger the cameras with a Stanford Research Systems Model DG535 digital delay generator. A schematic of the experimental setup is shown in Fig. 3. Many settings and arrangements required optimization. This process is discussed in the following sections, addressing tailoring the experimental setup to improve diagnostic efficiency for reduced material consumption, and tailoring the setup to minimize the presence of noise in the optical data collected.

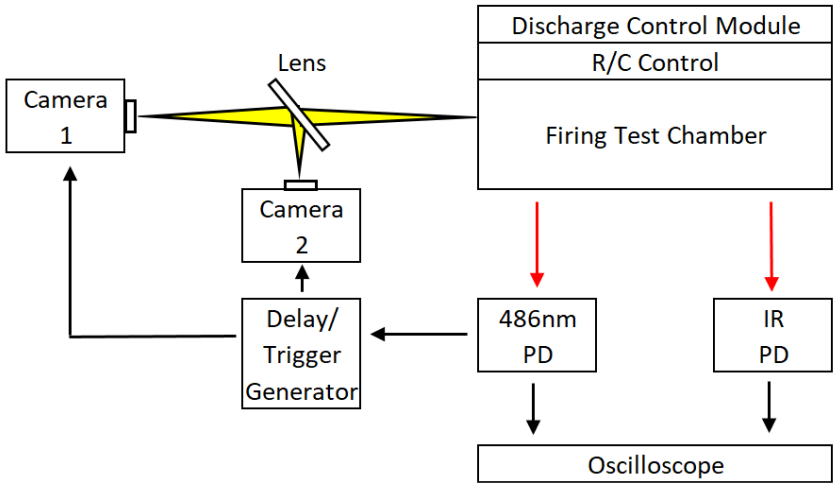

Fig. 3 Experimental schematic of the ESD system and additional diagnostics

3. Optimization of Experimental Parameters

3.1 ESD-Related Settings

The first issue we investigated was an extremely noisy discharge waveform and erroneous perception of discharge magnitude, or the "false peaks" phenomenon. This could occur when discharging at high voltages (particularly above 10 kV). Thus, all efforts were made to avoid testing at voltages above 10 kV. When increasing the test energy, it is suggested to alter the capacitance, rather than the discharge voltage, whenever voltages exceeding 10 kV are necessary. This additionally avoids an observed limiting behavior, where the theoretical maximum discharge voltage obtainable with a particular capacitor was greater than the actual voltage the system could reach.

With the ESD device used, altering the resistance primarily served to improve the initial discharge waveform. For the purpose of this work, the resistance was kept at 0 Ω since discharge waveform attenuation was deemed an unnecessary complication in the data analysis process, since the discharge waveform attenuation occurs at such a fast timescale that it becomes irrelevant to potential particle ignition waveforms collected.

Due to the insulating effects caused by the Scotch-brand 3M tape used to secure the sample to the sample holder, issues in initiating the arc when attempting low-energy discharges needed to be addressed. Double-sided carbon tape was found to more readily facilitate arcing. Thus, the carbon tape was placed on the top flat surface of the grounded sample holder. A small amount of the sample (roughly 15 mg depending largely on sample particle size) was then applied to the carbon tape and patted down. The sample was then subjected to the ESD. Due to the dispersive effect of the discharge on the sample particulate matter (regardless of sample ignition status), each prepared sample was only subjected to a single discharge before the tape was removed and a fresh sample was prepared to ensure consistency between tests.

Another issue addressed was an observed difficulty in initiating arcing due to the sample holder being too far away from the electrode. This was resolved by increasing the sample holder height to at least 75 mm; this arrangement was observed to consistently produce arcing for low-energy discharges of about 5 mJ or less. The sample stage was fixed at a distance of 75 mm from the floor of the firing chamber to the top of the inverted holder, as additional increases in height resulted in proportional increases in noise.

3.2 Diagnostic-Related Settings

The majority of the samples studied during the scope of this project consisted of Al, which produces the gas phase intermediate species aluminum monoxide (AlO) and fine alumina (Al_2O_3) nanoparticulates when undergoing combustion.[21] Thus, an Andover Corporation 486FSX10-50 AlO bandpass filter (486-nm center wavelength with 10-nm bandwidth) was added to the visible range PD. This tailored the visible data collection to detect the byproducts of aluminum sample combustion, while excluding other superfluous signals. It should be noted that although this particular filter does block IR radiation, this was not a concern since IR wavelength radiation was outside the detection range of the visible wavelength PD the filter was fastened to.

Steps needed to be taken to avoid signal saturation. Though lowering the PD gain would ostensibly solve this problem, tailoring the gain factor was necessary for

minimizing noise in the data collection, and thus could not be optimized to address saturation. The primary method of preventing saturation was thus introducing optical filters to the PDs experiencing signal saturation to lower the intensity of the signal detected. The IR range PD, being the only PD experiencing saturation, was equipped with a ThorLabs NENIR05A-C neutral density absorptive IR filter with a 0.5 optical density to dampen the entire range of detected radiation uniformly. When installing broadband filters, it was necessary to compare filter manufacturer transmissivity curves to the range of detection of the PDs, ensuring that the filter does not inadvertently truncate the PD wavelength sensitivity range.

PDs and any accompanying optical filters were attached to a translation stage, so that they can easily be moved to allow the ESD firing test chamber door to be opened and relocated to their initial location once the door is closed. When the door was closed, the PD stage was set to be approximately 2.25 inches from the ESD chamber door.

Fiber optic cables were forgone to limit the potential sources of electrical interference or noise in the system. If fiber optics were to become necessary for any reason, the effect of their introduction on the potential noisiness of the system would need to be experimentally determined and accounted for in the data collection and analysis processes.

An additional difficulty was missing signal confirmation of combustion, despite physical evidence of combustion having taken place. By preliminarily maximizing the data collection time on the oscilloscope, an expected reaction duration range could be established for a particular sample or group of samples, allowing for more informed decisions regarding temporal scaling to be made afterward.

A number of steps were taken to minimize the presence of noisy oscillatory behavior in the optical signal collected. With regards to data analysis and postprocessing procedures, a 10-point boxcar averaging approach was taken and, when sufficient sample material was available to test, an average of multiple (typically three) waveforms was taken for each trial. With regard to hardware arrangements to minimize noise, the first step was placing shielding around electrical equipment, such as the delay generator and oscilloscope, to avoid introducing noise to the system, essentially forming a Faraday cage around the potentially sensitive electronics. As a second step, an oscilloscope that has the ability to tailor the channel impedance was used. For the channel linked to the visible range PD, it was necessary to set the channel impedance at 1 MΩ. The IR range PD channel, meanwhile, was optimized at 50 Ω. The third step was tailoring the PD gain factor while running a blank trial. By improving the inherently messy short-timescale electrical discharge waveform, as shown in Fig. 4, the longer-

duration combustion waveform was also optimized indirectly. This electrical noise was most prominent when little or no particle combustion occurred.

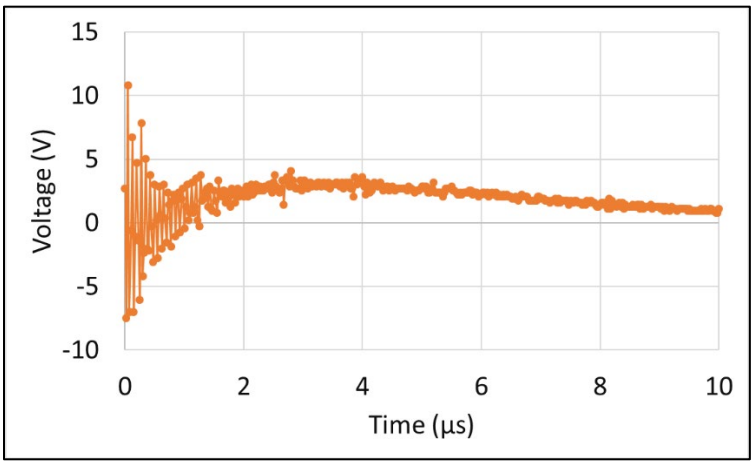

Fig. 4 PD signal from the ESD generated on blank carbon tape at 625 mJ

Additionally, the triggering threshold of the oscilloscope needed to be tailored. The threshold needed to be high enough to initiate data collection when the PDs detected the discharge, yet low enough to prevent triggering prematurely on electrical noise caused by the system or the mechanical discharge switch. Alternatively, the PD sampling frequency was lowered when the observed noise could not be minimized in any other way. This served as a form of built-in data smoothing, prior to the 10-point boxcar averaging performed in postprocessing, and was particularly useful during the noisy initial approximately 0.3 ms when the discharge was taking place. A moderate 300-kHz sampling frequency was used for most tests, only necessitating attenuation to 100 kHz when discharging at energies above approximately 100 mJ (an experimentally determined tentative datum). However, the duration of the noisy initial discharge signal was typically significantly shorter than the definitive optical signal observed during combustion. While taking steps to minimize noise ensures additional diagnostic accuracy regarding behavioral characteristics during combustion, the presence of some noise in the system during the short-timescale discharge did not pose significant issues in distinguishing between the short duration discharge and the much longer timescale combustion events.

4. Summary of Calibrated Experimental Settings

The experimental apparatus settings employed needed to be tailored based on the energy level of the discharge used, as a significant change in discharge energy resulted in noise, saturation, or detection issues when attempting to maintain consistent settings throughout the experimentation process. The high-speed cameras were fixed at 10 kFPS with a 1-μs shutter, as the videos for this preliminary study served no diagnostic purposes and were only intended for visualization of the combustion events. The delay generator, used to trigger the camera assembly once a signal from the visible range PD was detected, was set to simultaneously trigger both cameras (further triggering configurations are discussed later). Additionally, the detection sensitivity of the delay generator external PD trigger was maintained at 0 V during the course of this research. The experimentally determined settings of the remaining equipment are summarized in Table 1. The discharge energies were determined by Eq. 1, with E being energy in joules (J), C representing capacitance in farads (F), and V the discharge voltage in volts (V).

$$E = \frac{1}{2} C \times V^2 \tag{1}$$

Table 1 Experimental apparatus settings under different discharge conditions

Experimental Apparatus	Discharge Energy (J)	Settings
Electrostatic Discharge (ESD) Device	0.004 - 0.009:	0 Ω, 100 pF, 9 kV - 13.5 kV
	0.010 - 0.015:	0 Ω, 250 pF, 9 kV - 11 kV
	0.016 - 0.033:	0 Ω, 500 pF, 8 kV - 11.5 kV
	0.036 - 0.100:	0 Ω, 2000 pF, 6 kV - 10 kV
	0.101 - 0.211:	0 Ω, 0.01 μF, 4.5 kV - 6.5 kV
	0.245 - 0.605:	0 Ω, 0.01 μF, 7 kV - 11 kV
	$0.625 \sim 1.225$:	0 Ω, 0.05 μF, $5\ \mathrm{kV} \sim 7\ \mathrm{kV}$
	10.563:	0 Ω, 0.5 μF, 6.5 kV
300 - 1100 nm visible range photodiode with 486 nm AlO filter	0.004 - 0.009:	$10^4 \times 3$ gain factor, 300 kHz sampling frequency
	0.010 - 0.015:	$10^4 \times 3$ gain factor, 300 kHz sampling frequency
	0.016 - 0.033:	$10^4 \times 1$ gain factor, 300 kHz sampling frequency
	0.036 - 0.100:	$10^3 \times 3$ gain factor, 300 kHz sampling frequency
	0.101 - 0.211:	$10^3 \times 1$ gain factor, 100 kHz sampling frequency
	0.245 - 0.605:	$10^2 \times 3$ gain factor, 100 kHz sampling frequency
	$0.625 \sim 1.225$:	$10^2 \times 3$ gain factor, 100 kHz sampling frequency
	10.563:	$10^2 \times 1$ gain factor, 100 kHz sampling frequency
800 - 1800 nm IR range photodiode with NENIR05A-C filter	0.004 - 0.009:	$10^4 \times 3$ gain factor, 300 kHz sampling frequency
	0.010 - 0.015:	$10^4 \times 3$ gain factor, 300 kHz sampling frequency
	0.016 - 0.033:	$10^4 \times 3$ gain factor, 300 kHz sampling frequency
	0.036 - 0.100:	$10^4 \times 1$ gain factor, 300 kHz sampling frequency
	0.101 - 0.211:	$10^3 \times 3$ gain factor, 100 kHz sampling frequency
	0.245 - 0.605:	$10^3 \times 1$ gain factor, 100 kHz sampling frequency
	$0.625 \sim 1.225$:	$10^3 \times 1$ gain factor, 100 kHz sampling frequency
	10.563:	$10^2 \times 3$ gain factor, 100 kHz sampling frequency
Digital storage oscilloscope	0.004 - 0.009:	10 ms data collection gate, 438 mV trigger threshold
	0.010 - 0.015:	10 ms data collection gate, 375 mV trigger threshold
	0.016 - 0.033:	10 ms data collection gate, 375 mV trigger threshold
	0.036 - 0.100:	10 ms data collection gate, 375 mV trigger threshold
	0.101 - 0.211:	10 ms data collection gate, 188 mV trigger threshold
	0.245 - 0.605:	10 ms data collection gate, 125 mV trigger threshold
	$0.625 \sim 1.225$:	10 ms data collection gate, 813 mV trigger threshold
	10.563:	10 ms data collection gate, 1.0 V trigger threshold

5. Recommended Criteria for Determining Go/No-Go

The primary advance of this project was the development of objective criteria for determining a sample's ignition status. This was achieved by comparing the PD traces of a representative sensitive sample studied with consistent minimum-energy settings, thus serving three purposes: the minimum discharge energy required to ignite the sample would produce negligible interfering effects on any combustion emission detected, the energetic reaction when the sample combusts could more easily be distinguished from its no-go counterpart, and the presence of significant changes in the PD traces would be solely the result of ignition, rather than differing experimental conditions. As a crucial step to remove subjectivity from this diagnostic procedure, the PD traces collected were the only diagnostic tool used to confirm combustion. Figure 5 compares the differences in the observed optical emission when combustion does or does not occur, as determined by the application of the developed objective criteria, after subjecting a highly sensitive sample to low-energy ESDs. Since both trials were conducted under identical experimental conditions, the presence of a significant increase in optical emission during one trial validated that this methodology can objectively identify sample ignition.

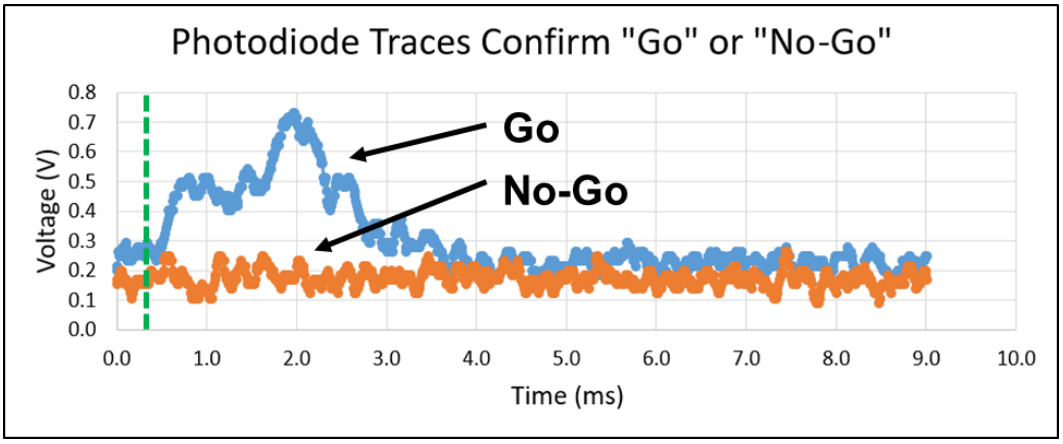

Fig. 5 Comparison of "go" vs. "no-go" optical signals for a highly sensitive sample; emission observed at times greater than 0.3 ms (green dashed line) indicates successful particle ignition/combustion ("go")

A 0.3-ms threshold was established after which the presence of significant optical emission was taken to be an indication that the sample under observation had ignited. Likewise, the lack of any such signal was indicative that the sample had not ignited. The determination of this threshold was made following a lack of any extended-timescale signal when subjecting an insensitive sample to a massive 10.5 J discharge. The 10.5-J discharge emission, approaching the testing limit of the experimental apparatus, had completely dispersed by 0.2 ms. It could thus be

reasonably inferred that the significantly smaller discharges anticipated during testing and their accompanying noise would have adequate time to disperse before the 0.3-ms threshold was exceeded. Furthermore, the discharge energy threshold at which a sample begins to consistently ignite is used to determine that sample's electrostatic sensitivity. Further experimentation to study the optical nuances of this novel procedure would be necessary to solidify any cutoffs established, gain insight into early timescale interactions, and to develop a better understanding of a sample's behavior as the discharge energy begins to approach the consistent ignition threshold.

6. Application of Methodology to Samples of Interest

Two samples, both comprising 110-nm aluminum nanoparticles (nano-Al) and graphene oxide (GO), were studied during the course of this research. Figure 6 shows scanning electron microscopy (SEM) images of the nano-Al powder (left) and GO sheets (right). SEM images were obtained using a Hitachi S4700 field emission scanning electron microscope operating under 5 kV.

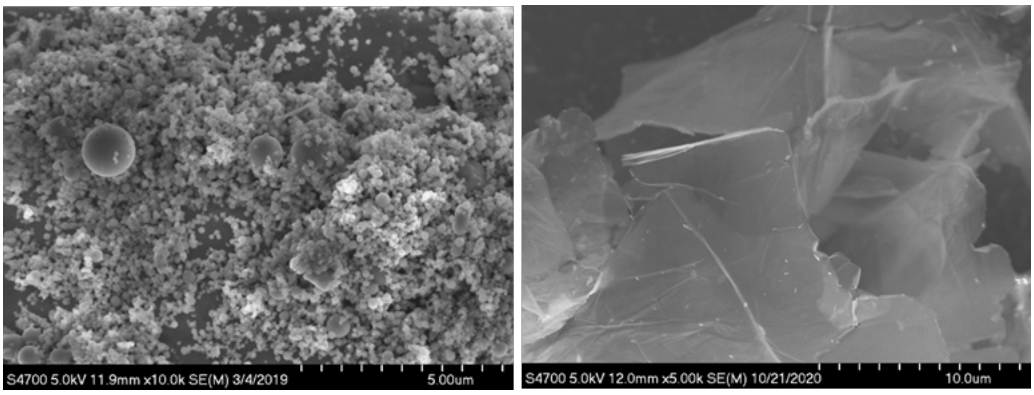

Fig. 6 SEM images of commercial nano-Al (left) and commercial GO (right)

The first sample studied was an inhomogeneous, physically mixed combination of the nano-Al and GO. In this sample, the GO was erratically dispersed throughout, rather than coating the nano-Al particles uniformly. Upon ESD analysis, using the described objective criteria, it was discovered that this sample exhibits substantial electrostatic sensitivity. Whereas conventional organic additives are usually classified as "electrostatically sensitive" if ignition occurs at or below 100 mJ of discharge energy,[2] the physically mixed nano-Al+GO sample ignited consistently at 5 mJ for all three shots. When subjected to a 4-mJ discharge, the sample ignited once out of the three shots. Figure 7 is a snapshot from the high-speed video depicting the sample igniting during a 10-mJ discharge, where the dispersed

particles can be seen burning after 3.0 ms. The particles are ejected into the air above the sample holder by the shockwave formed by the ESD.[13]

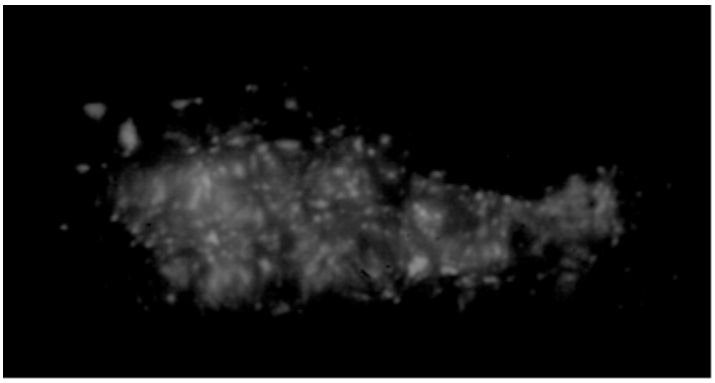

Fig. 7 Snapshot from the high-speed video of physically mixed nano-Al+GO sample burning 3.0 ms after ESD ignition at 10 mJ (picture has been cropped and the brightness/contrast adjusted)

Figure 8 compares the AlO and IR signal observed for all shots taken. The top orange PD traces depict the average of all three igniting 5-mJ discharges, the gray traces are from the single 4-mJ discharge that ignited, and the blue traces show the average of the two 4-mJ discharges that failed to ignite. In comparing the 4- and 5-mJ ignition traces, it is evident that an increase in discharge energy results in increased magnitude for the combustion emission. Furthermore, while the 4-mJ discharge that ignited experiences peak initial and secondary combustion intensities at roughly 1 and 2 ms, respectively, the 5-mJ discharge ignition exhibits a noticeably extended duration of reaction. For the 5-mJ discharge, the time to peak initial and secondary combustion intensities have increased to roughly 3 and 5.5 ms, respectively. Following the recommended objective criteria established, the physically mixed nano-Al+GO sample's sensitivity was determined to be 5 mJ, with further study of the reaction dynamics taking place at the 4-mJ discharge level continuing in the future.

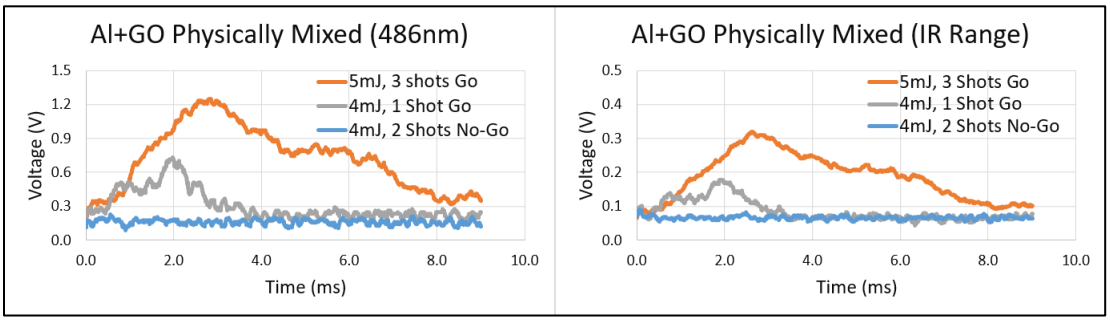

Fig. 8 AlO (left) and IR (right) PD traces for the physically mixed nano-Al+GO sample

The second sample studied was formulated so that the GO more completely coated the nano-Al particles. Figure 9 shows SEM images of the GO-coated nano-Al at 20,000× (left) and 50,000× (right) magnification. The distinct morphology of the sample particles is due to the GO coating, forming a much more homogeneous mixture than the previous physically mixed sample.

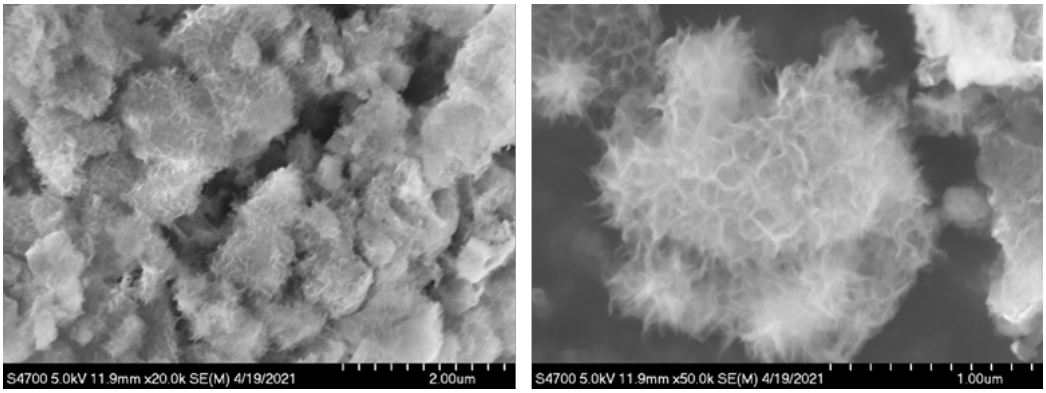

Fig. 9 SEM images of GO-coated nano-Al at 20,000× (left) and 50,000× (right)

The effect of this coating of GO resulted in an extreme decrease in electrostatic sensitivity. When shot with a 5-mJ discharge for comparison, the GO-coated Al sample did not ignite. The discharge energy was gradually increased until finally the sample was subjected to a 10.563-J discharge. Even when exposed to this massive ESD, the sample still did not undergo any combustion reaction. The PD traces from the 5-mJ and 10.563-J discharges are shown in Fig. 10. It is clear that no significant optical signal was detected after 0.3 ms, even for the 10.563-J discharge. This complete absence of post-discharge optical emission verifies that the sample exhibited much lower electrostatic sensitivity as a result of the GO coating. Figure 11, a snapshot of the high-speed video acquired during the 10.563-J test, depicts the discharge emission after 30 μs. The black spots seen inside the discharge are the dispersed particles ejected from the tape that were not burning. Some small, uncoated nano-Al particles may be burning at these very earlier times (see circled area), but it is clear that most do not.

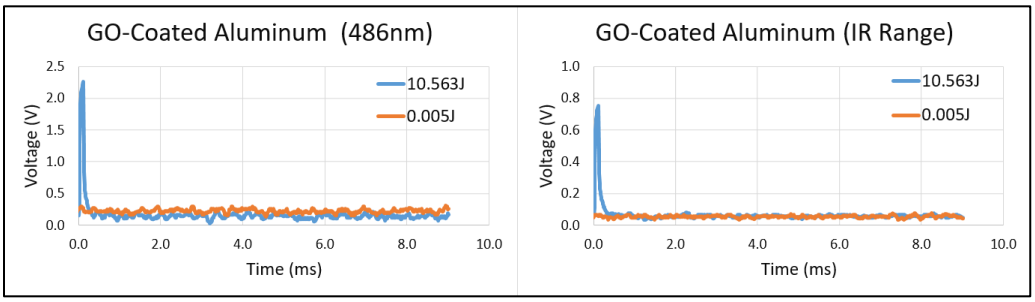

Fig. 10 AlO (left) and IR (right) PD traces for the GO-coated nano-Al sample

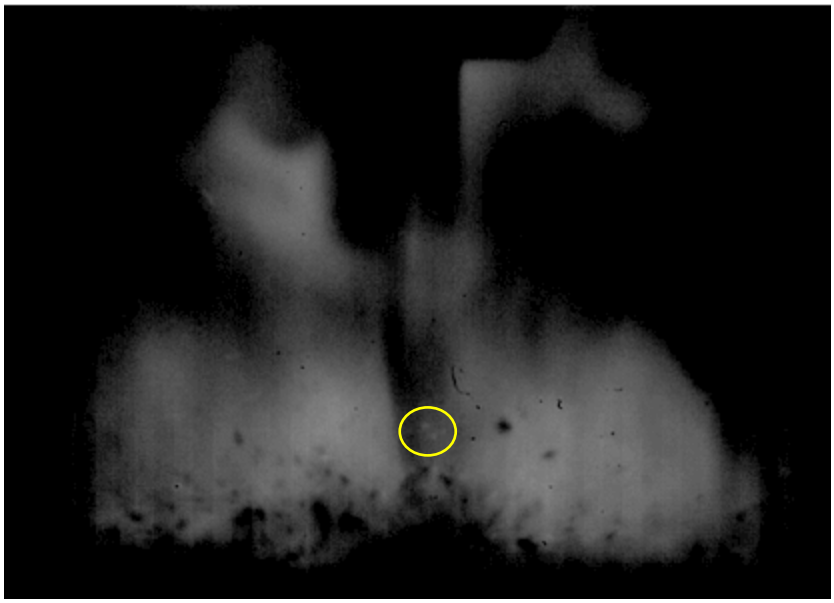

Fig. 11 Snapshot from the high-speed video of GO-coated nano-Al particles being ejected into the air 30 µs after being subjected to a 10.5-J discharge; the ejected particles appear black against the residual discharge emission since they are not burning, while a few smaller particles inside the yellow circle may be burning (picture has been cropped and the brightness/contrast adjusted)

7. Discussion and Conclusions

We have demonstrated that changing the synthesis/processing method can significantly influence the electrostatic sensitivity of a metal composite material. A hypothesized cause of the GO-coated nano-Al sample's resistance to electrostatic ignition is a previously observed phenomenon discussed in work by Collins et al.[22] The samples used in that research were composed of 3.0- to 4.5-µm aluminum particles loosely wrapped in graphene nanoplatelets. When subjected to a 100-mJ discharge, the samples failed to ignite. Upon further study, it was found that the graphene nanoplatelets redirected the discharge energy around the reactive aluminum interior, thereby preventing the aluminum from becoming excited and igniting. Given the similar material composition between the nanoplatelet samples and the GO-coated samples used in the current research, especially noting the difference in the efficiency of the GO coating compared to the physically mixed sample, it is hypothesized that the increased resistance to electrostatic ignition is caused by the same mechanism.

The correlation between conductivity and electrostatic sensitivity is also discussed in the detailed study by Weir et al.[5] In that work, it was found that only the most conductive sample tested, a mixture of micron-sized AL and Cu_2O, experienced ignition from an ESD stimulus. By assessing the conductivities of the samples

studied in this work in comparison to the minimum ignition energies observed, it may be possible to determine if a causal relationship exists between the two for this class of materials as well.

8. Future Work

Moving forward, continued work for this research includes the application of the novel objective go/no-go criteria developed for determining the minimum ignition energy of metallic additives to the study of other reactive materials being investigated as novel energetic additives for enhanced performance. Additional analysis of the sample composition and properties may lead to a better understanding of their effect on early timescale discharge interactions, reaction dynamics, and electrostatic sensitivity as a whole.

Once the objective measurement process has been refined, the development of a multilevel electrostatic sensitivity testing regime may commence. Currently, novel organic explosives undergo ESD sensitivity testing before and after formulation. Their electrostatic sensitivity is compared to that of the conventional explosive RDX, and they are approved for further testing or development if they are found to be less than or equally sensitive. With the introduction of electrostatically sensitive metallic additives, it is necessary to develop a preliminary testing phase prior to scale-up, formulation, and large-scale performance testing. A proposed algorithm for a two-step electrostatic sensitivity testing regime is presented in Fig. 12.

During the first step, the development of the novel metal additive would take place. Subsequently, a small sample would need to demonstrate less than or equal electrostatic sensitivity in comparison to some baseline insensitive material such as micron-sized Al particles, which are currently approved for use in aluminized explosive formulations. After passing the first phase of testing (to include impact and friction sensitivity testing in addition to ESD sensitivity determination), scale-up of the metal additive can be performed in order to begin formulation development (ensuring compatibility with formulation ingredients). Comparison of the resultant formulation's electrostatic sensitivity to conventional RDX may then take place. Only after both phases of testing may the novel energetic material be approved for further testing or development.

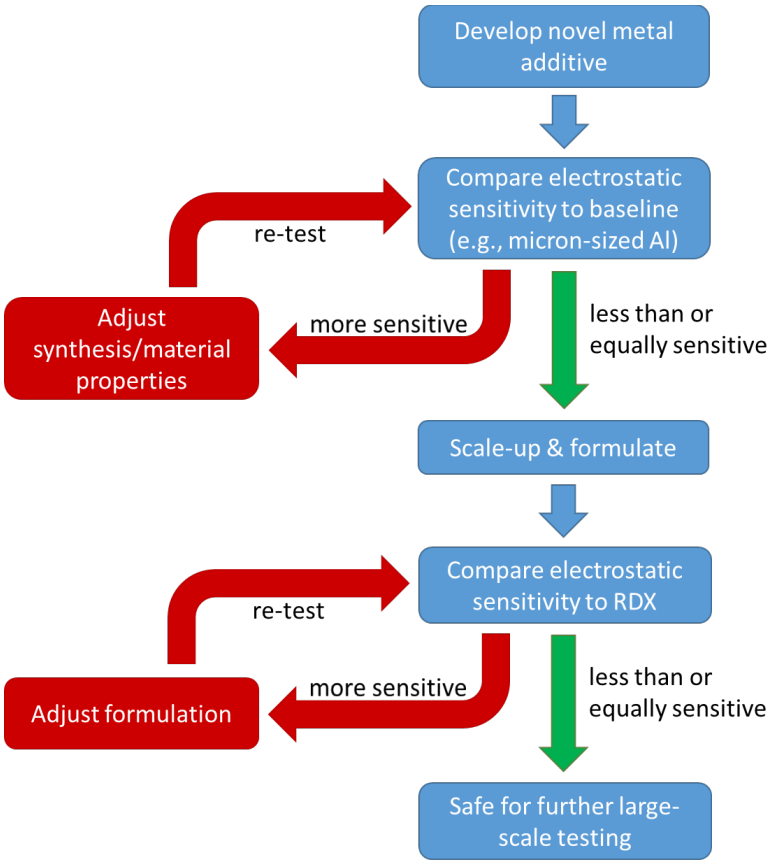

Fig. 12 Proposed multistep electrostatic sensitivity testing regime for novel metal additives

9. References

1. Jiang Y, Deng S, Hong S, Zhao J, Huang S, Wu C-C, Gottfried JL, Nomura K-i, Li Y, Tiwari SC, Kalia RK, Vashishta P, Nakano A, Zheng X. Energetic performance of optically activated aluminum/graphene oxide composites. ACS Nano. 2018;12:11366–11375.

2. Department of Defense (US). Safety and performance tests for the qualification of explosives (high explosives, propellants, and pyrotechnics). Department of Defense (US); 1982. Report No.: MIL-STD-1751A.

3. Munson CA, Roos BD, Johnson EC, Pridgeon LA, Piatt TL, Spangler KY, Aubert SA. Small-scale testing of HQ formulations: insensitive replacements for octol. Army Research Laboratory (US); 2015. Report No.: ARL-TR-7221.

4. Collins ES, Gottfried JL, Johnson EC. New method for quantifying ignition sensitivity from electrostatic discharge. Army Research Laboratory (US); 2015 May. Report No.: ARL-TN-0675.

5. Weir C, Pantoya ML, Ramachandran G, Dallas T, Prentice D, Daniels M. Electrostatic discharge sensitivity and electrical conductivity of composite energetic materials. J Electrostat. 2013;71(1):77–83.

6. Steelman R, Clark B, Pantoya ML, Heaps RJ, Daniels MA. Desensitizing nano powders to electrostatic discharge ignition. J Electrostat. 2015;76:102–107.

7. Poper KH, Collins ES, Pantoya ML, Daniels MA. Controlling the electrostatic discharge ignition sensitivity of composite energetic materials using carbon nanotube additives. J Electrostat. 2014;72(5):428–432.

8. Weir C, Pantoya M, Daniels M. The role of aluminum particle size in electrostatic ignition sensitivity of composite energetic materials. Combust Flame. 2013;160:2279–2281.

9. Beloni E, Dreizin EL. Ignition of aluminum powders by electro-static discharge. Combust Flame. 2010;157(7):1346–1355.

10. Williams RA, Dreizin EL, Beloni E. Ignition of metal powder layers of different thickness by electrostatic discharge. J Propul Power. 2012;28(1):132–139.

11. Williams RA, Patel JV, Dreizin EL. Ignition of fully dense nanocomposite thermite powders by an electric spark. J Propul Power. 2014;30(3):765–774.

12. Monk I, Williams R, Liu X, Dreizin EL. Electro-static discharge ignition of monolayers of nanocomposite thermite powders prepared by arrested reactive milling. Combust Sci Technol. 2015;187(8):1276–1294.

13. Huang C, Schoenitz M, Dreizin EL. Displacement of powders from surface by shock and plasma generated by electrostatic discharge. J Electrostat. 2019;100:103353.

14. Huang C, Schoenitz M, Dreizin EL. Ignition of zirconium powders placed near an electrostatic discharge. Combust Flame. 2021;226:1–13.

15. Pichot V, Comet M, Miesch J, Spitzer D. Nanodiamond for tuning the properties of energetic composites. J Hazard Mater. 2015;300:194–201.

16. Gibot P, Goetz V. SnO2-polyaniline composites for the desensitization of Al/SnO2 thermite composites. J Appl Polym Sci. 2020;137(32).

17. Goetz V, Gibot P, Spitzer D. Spark sensitivity and light signature mitigation of an Al/SnO2 nanothermite by the controlled addition of a conductive polymer. Chem Eng J. 2022;427:131611.

18. Sippel T, Son S, Risha G, Yetter R. Combustion and characterization of nanoscale aluminum and ice propellants. 44th AIAA/ASME/SAE/ASEE Joint Propulsion Conference & Exhibit; 2008; Hartford, CT.

19. Dean SW, McNesby KL, Benjamin RA. High dynamic range imaging of energetic events. Joint Army Navy NASA Air Force (JANNAF) 41st Propellant and Explosives Development and Characterization (PEDCS); 2018 Dec 10–13; Vancouver, WA.

20. Densmore JM, Homan BE, Biss MM, McNesby KL. High-speed two-camera imaging pyrometer for mapping fireball temperatures. Appl Opt. 2011;50(33):626–6271.

21. Wainwright ER, Dean SW, De Lucia Jr. FC, Weihs TP, Gottfried JL. Effect of sample morphology on the spectral and spatiotemporal characteristics of laser-induced plasmas from aluminum. Appl Phys A. 2020;126:83.

22. Collins ES, Skelton BR, Pantoya ML, Irin F, Green MJ, Daniels MA. Ignition sensitivity and electrical conductivity of an aluminum fluoropolymer reactive material with carbon nanofillers. Combust Flame. 2015;162(4):1417–1421.

List of Symbols, Abbreviations, and Acronyms

Al	aluminum
AlO	aluminum monoxide
C	carbon
CNT	carbon nanotube
Cu_2O	copper oxide
DOD	Department of Defense
ESD	electrostatic discharge
GO	graphene oxide
H	hydrogen
IR	infrared
Mg	magnesium
N	nitrogen
O	oxygen
PD	photodiode
RDX	cyclotrimethylene trinitramine
SEM	scanning electron microscopy
Ti	titanium
Zr	zirconium

1 (PDF)	DEFENSE TECHNICAL INFORMATION CTR DTIC OCA
1 (PDF)	DEVCOM ARL FCDD RLD DCI TECH LIB
5 (PDF)	DEVCOM ARL FCDD RLW WA J GOTTFRIED E WAINWRIGHT L GIRI K NAUDE C-C WU